

Test of replica theory: Thermodynamics of two-dimensional model systems with quenched disorderSimon Bogner,¹ Thorsten Emig,¹ Ahmed Taha,² and Chen Zeng²¹*Institut für Theoretische Physik, Universität zu Köln, Zùlpicher Straße 77, 50937 Köln, Germany*²*Department of Physics, George Washington University, Washington, DC 20052, USA*

(Received 9 September 2003; published 22 March 2004)

We study the statistics of thermodynamic quantities in two related systems with quenched disorder: A $(1 + 1)$ -dimensional planar lattice of elastic lines in a random potential and the two-dimensional random bond dimer model. The first system is examined by a replica-symmetric Bethe *Ansatz* (RBA) while the latter is studied numerically by a polynomial algorithm which circumvents slow glassy dynamics. We establish a mapping of the two models which allows for a detailed comparison of RBA predictions and simulations. Over a wide range of disorder strength, the effective lattice stiffness and cumulants of various thermodynamic quantities in both approaches are found to agree excellently. Our comparison provides a detailed quantitative confirmation of the replica approach and renders the planar line lattice a unique testing ground for concepts in random systems.

DOI: 10.1103/PhysRevB.69.104420

PACS number(s): 75.10.Nr, 65.60.+a, 02.60.Pn

I. INTRODUCTION

Quenched disorder is common to many condensed-matter systems. Examples include spin glasses,¹ elastic structures in a random environment² or mesoscopic electronic systems.³ In spite of a large volume of theoretical and experimental work on glasses these systems still pose interesting challenges. On the theoretical side, much of the studies have focused on phase diagrams, the existence of phase transitions and their critical behavior. But even if the equilibrium phases are known, thermodynamic quantities are in general not accessible. Slow glassy equilibration due to the presence of many metastable states on large length scales is the main obstacle to the numerical and experimental study of disordered systems. There exist, however, a number of well-tested analytical tools to study the equilibrium properties. Common to basically all approaches is that they rely on the introduction of replicas in order to reestablish translational invariance. The replicated system is then usually studied by a renormalization-group (RG) approach⁴ or a Gaussian variational *Ansatz*⁵ (GVA) since perturbation theory completely fails. The first method is designed to yield the effective pinning potential at large length scales. The latter approach aims at constructing a Gaussian trial Hamiltonian which describes the glassy phase. The results of the RG approaches are, strictly speaking, valid only close to the upper critical dimension or close to a critical point where randomness becomes irrelevant. On the other hand, the GVA has to be combined with the concept of “replica symmetry breaking” which is not generally accepted for elastic structures in random media.² Although the results of both approaches are similar, the different underlying concepts indicate that the present general understanding of disordered systems is still incomplete. A more general qualitative picture was developed in form of the droplet theory for spin glasses.⁶ It provides a phenomenological scaling approach to static and dynamics properties of the spin-glass ordered phase. The properties of this phase are characterized in terms of connected clusters (droplets) of coherently flipped spins with minimal free energy. It would be desirable to have a detailed quantitative test

of this theory. Progress on numerical approaches as Monte Carlo simulations at finite temperatures was seriously hampered by the slow dynamics. Only recently novel power full polynomial algorithms became available for the study of large systems at any temperature.^{7,8}

On the experimental side, most of the effort was devoted to spin glasses and pinned vortex systems. Especially the latter class comprises a system which is accessible to exact both analytical methods and numerical algorithms. It is a randomly pinned planar vortex lattice that was highlighted by an experimental study of magnetic-flux lines threading through a thin film of the superconductor 2H-NbSe₂.⁹ For a certain class of two-dimensional (2D) random systems, including the flux line lattice, new promising approaches have been developed. For a planar lattice of noncrossing elastic lines pinned by disorder a replica Bethe *Ansatz* (RBA) can be employed, yielding exact results for thermodynamic quantities and their cumulants.¹⁰⁻¹² For the related⁸ random bond dimer model the partition function can be calculated exactly by a polynomial algorithm^{14,15} without the need to run slow relaxation dynamics. Therefore, both methods are perfectly suited to overcome the drawbacks of the above-mentioned approaches. However, there are also limitations to the RBA and the dimer simulations. The first does not allow to compute correlation functions whereas in the latter the choice of parameters of the related line-lattice model is restricted, e.g., only one particular density of lines can be simulated.

The aim of the present work is to show that the thermodynamics of the two studied model systems provide ideal environments for a quantitative test of replica theory including replica symmetry breaking and analytical continuation. Here the 2D model systems can be considered counterparts of exactly solvable 1D quantum systems which have advanced the understanding of strongly correlated systems in general. Our main result is that RBA and dimer model simulations agree so well that they prove each other to be reliable and thus allow to explore many questions in detail that had been inaccessible to date.

The rest of the paper is organized as follows. In the fol-

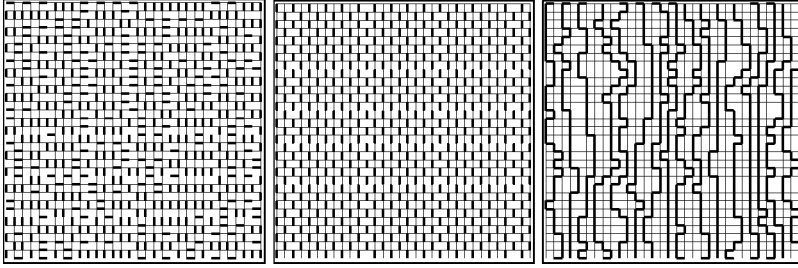


FIG. 1. Mapping of a dimer (left) to a line configuration (right) via XOR addition of the reference state (middle).

In the following section we introduce the line-lattice model and the dimer model, and explain their mutual relation and their connections to other models. In Sec. III we review briefly the replica Bethe *Ansatz* for the line system and summarize the results in the known limiting cases. We continue in Sec. IV with a detailed quantitative comparison of the Bethe *Ansatz* predictions for various thermodynamic quantities and the corresponding simulation data for the dimer model. To do so, the Bethe *Ansatz* equations are solved numerically outside the validity range of the previously studied limiting cases. We close with a summary and discussion of our results in Sec. V.

II. THE MODELS AND THEIR CONNECTIONS

A. Vortex system

We consider an ensemble of directed vortex lines confined to a plane at average distance $a \equiv 1/\rho$. The configurations of a single directed line are characterized by its position $x_i(z)$ since overhangs are forbidden. The preferred path of the line results from the competition between elastic energy, measured by the line tension g , the line interaction in form of a repulsive pair potential $U(x)$ that does not allow the lines to cross, and pinning by a random impurity potential. With a contact repulsion $U(x) = c\delta(x)$, $c \rightarrow \infty$, ensuring the non-crossing condition, the model remains generic¹³ and allows for the mapping to a discrete dimer model. Quenched disorder couples locally to the vortices via a random potential $V(\mathbf{r})$, which we assume to have zero mean and short-range correlations

$$\overline{V(\mathbf{r})V(\mathbf{r}')} = \Delta \delta_{\xi_d}(\mathbf{r} - \mathbf{r}'). \quad (1)$$

Whenever the disorder correlation length ξ_d is the smallest scale in the problem it can safely be set to zero. The total energy can be written as

$$H = \int dz \sum_i \left\{ \frac{g}{2} \left(\frac{dx_i}{dz} \right)^2 + c \sum_{i,j \neq i} \delta(x_i - x_j) + V(x_i, z) \right\}. \quad (2)$$

Throughout the paper, the disorder average will be denoted by $\overline{\dots}$ and the thermal average by $\langle \dots \rangle$.

B. Dimer model

The dimer model is defined as follows: Choose a subset (whose elements are called dimers) of the bonds on a square lattice with lattice constant b and linear size L such that each of the $L^2 = N$ lattice sites [labeled by (ij)] is touched by

exactly one of these dimers, see Figs. 1 and 3. A square lattice rotated by 45° with lattice constant $b/\sqrt{2}$ is formed by the centers of the bonds. Its $2N$ sites shall for convenience also be labeled by (ij) and it will be clear from the context if the original lattice or that of the bonds is parametrized. The reduced energy of one such complete covering D of $N/2$ dimers is defined by

$$H_d = \sum_{(ij) \in D} \epsilon_{ij} / T_d, \quad (3)$$

where the sum is over all dimers of D . The bond energies ϵ_{ij} are randomly drawn from a Gaussian distribution with zero mean and unit variance $\overline{\epsilon_{ij}\epsilon_{kl}} = \delta_{(ij),(kl)}$. T_d is the dimer temperature and measures the strength of disorder. The implementation of the polynomial algorithm^{14,15} (with exponent ≈ 2) on a 32-processor cluster allows to compute thermodynamic quantities numerically exactly—as opposed to, e.g., Monte Carlo sampling—for sizes up to $L = 512$ at typically 6000 disorder configurations within a CPU time of days. Merely the measurement of the specific heat in Sec. IV D is not covered by the polynomial algorithm. Thermal fluctuations have to be computed from explicitly sampling over a representative set out of $\exp(NG/\pi)$ possible dimer coverings,¹⁶ again for up to 6000 disorder configurations. This gives, however, also reliable results for sizes up to $L = 256$. The typical accuracy of numerical data at the given number of disorder samples is $\approx 10^{-5}$. For further details of the algorithm for the simulation of the dimer model see, e.g., Ref. 7.

C. Connections

These two apparently diverse models are closely related. The random bond dimer model can be mapped onto an array of lines that interact via a hard-core repulsion, preventing any line crossing. In Fig. 2 this mapping and the connections to related models are sketched. From the dimer model (A) on top, the discrete lattice version of the line model (C) can be reached directly or via the intermediate random solid-on-solid (SOS) model (B). Both the SOS model and the discrete lines have their continuous counterparts—in the bottom line of the sketch—that can be treated analytically: The two-dimensional random sine-Gordon (RSG) model (D) (being equivalent to the random-field XY model without vortices) and the continuum $(1+1)$ -dimensional elastic lattice of directed lines (E). The parameters and observables of the isotropic dimer model and its version with a height profile (SOS) can be expressed in terms of the anisotropic vortex-

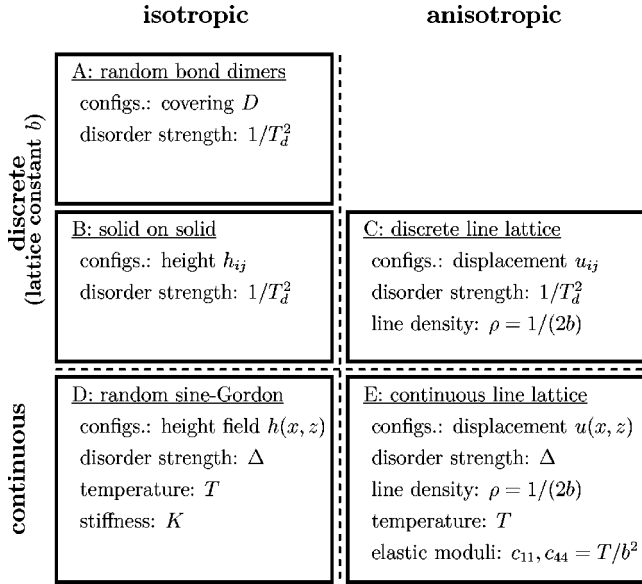


FIG. 2. Overview of the models introduced in the text, showing their degrees of freedom and parameters. *Top*, discrete models; *bottom*, continuous models; *left*, isotropic models; *right*, anisotropic models.

line lattice. In the following we describe the relations between the above-mentioned models in detail. We start the tour through the mapping table of Fig. 2 from the dimer model (A) with the dimer temperature T_d as the only control parameter. The discrete line lattice can be reached easily via the following map.

(AC). Add a given dimer pattern and a regular reference dimer covering as given in the middle of Figs. 1 and 3 with an “exclusive or” (XOR) operation. Only if a given bond is covered by either the dimer pattern or the reference pattern it shall be covered in the resulting line configuration, which will be noncrossing lines at average density $\rho = 1/(2b)$. A resulting line-lattice configuration is shown in the right part of Figs. 1 and 3. For the summed energies of all covered bonds in the respective configurations it holds

$$H_1(\{\epsilon'_{ij}\}) = H_d(\{\epsilon_{ij}\}) + H_{\text{ref}}(\{\epsilon'_{ij}\}). \quad (4)$$

Here and in the following, the subscript “ d ” stands for quantities of the dimer model, while line-lattice quantities are denoted by the subscript “ l .” $\{\epsilon_{ij}\}$ stands for a given distribution of random energies on all of the bonds of the dimer model while the set of random energies $\{\epsilon'_{ij}\}$ are defined as $\epsilon'_{ij} = -\epsilon_{ij}$ on the occupied bonds of the reference pattern and $\epsilon'_{ij} = \epsilon_{ij}$ elsewhere. If the original random bond energies $\{\epsilon_{ij}\}$

are distributed symmetrically with zero mean, so are the bond energies $\{\epsilon'_{ij}\}$ defining the discrete line-lattice model.

(AB). A discrete height profile $\{h_{ij}\}$ can be assigned to every plaquette of the square lattice in the following way:¹⁷ Every bond is given a sign ± 1 such that when going through rows or columns of plaquettes the sign of the crossed bonds alternates. Starting at a given plaquette with arbitrary height, one moves to the neighboring plaquettes and adds to the height $+3$ times the bond sign if the crossed bond is covered by a dimer, or -1 times the bond sign if it is not. The resulting numbers define a path-independent height profile $\{h_{ij}\}$, see Fig. 3 for an example.

(BC). Define a new discrete height profile $\{H_{ij}\}$ on each plaquette by subtracting the height profile $\{h_{ij}^{\text{ref}}\}$ associated with the reference dimer covering, cf. the middle part of Fig. 3,

$$H_{ij} \equiv h_{ij} - h_{ij}^{\text{ref}}. \quad (5)$$

The profile $\{H_{ij}\}$ is then quantized in steps of width 4. Plaquettes of constant H form domains of average width $2b$ that may be numbered by k . The domains are separated by domain walls which can be considered as directed lines. Next, we introduce the displacements $u_k(i)$ of these domain walls from their perfectly aligned positions where $i = 1, \dots, L$ and $j = 2k$. As illustrated in Fig. 4, the line displacements are determined by the height profile, leading to

$$u_k(i) = \frac{h_{ij}^{\text{(left)}} + h_{ij}^{\text{(right)}} - 1}{4}. \quad (6)$$

This notation indicates that in each row i the heights h_{ij} on the plaquettes left and right to the displaced line have to be used. It is important to keep in mind that the mapping to a displacement field makes sense only for a well-defined initial configuration of the domain walls implying a *fixed* density. In the grand canonical ensemble induced by the sum over dimer configurations, $u_k(i)$ is a good degree of freedom only for the configurations corresponding to the mean line density $\rho = 1/(2b)$, which, however, carry the dominant weight in the thermodynamic limit where the density distribution is sharply peaked.

(CE). In a continuum formulation each individual line can be considered as a directed polymer with energy $(g/2) \int dz \{ \partial_z x_i(z) \}^2$ and line tension g . If one includes the noncrossing condition imposed by the underlying dimer configurations and the coupling to disorder the continuum model is that introduced in Eq. (2). In a second step this system can be cast into the form of a two-dimensional elastic system. We define a continuous displacement field $u(\mathbf{r})$ so that the line

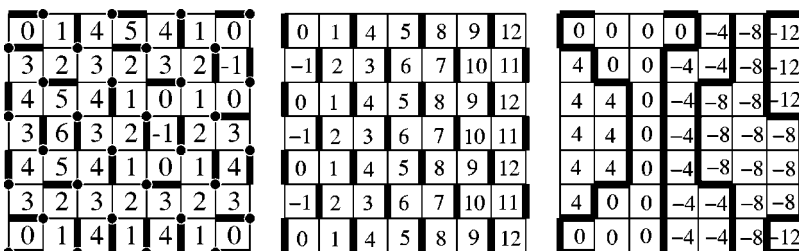
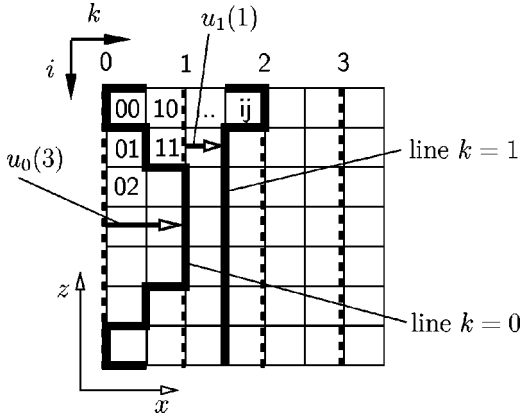


FIG. 3. Dimer covering (left), reference state (middle), and line configuration (right), with height profiles h_{ij} (left), h_{ij}^{ref} (middle), and H_{ij} (right).

FIG. 4. Illustration of displacements $u_k(i)$ in the discrete model.

positions are $x_i(z) = ia + u(ia, z)$. If we include the line interaction in the elastic energy, the Hamiltonian for fluctuations on sufficiently large length scales can be written as

$$H_{\text{el}} = \int d^2\mathbf{r} \left\{ \frac{c_{11}}{2} (\partial_x u)^2 + \frac{c_{44}}{2} (\partial_z u)^2 + \rho(\mathbf{r}) V(\mathbf{r}) \right\} \quad (7)$$

with compression modulus $c_{11} = aU''(a)$, tilt modulus $c_{44} = g/a$, and line density $\rho(\mathbf{r}) = \sum_j \delta(x - x_j(z))$. The correlations of the random potential $V(\mathbf{r})$ are given by Eq. (1). The compression modulus is obtained in elastic approximation from the line interaction potential $U(x)$,

$$c_{11} = a \frac{\partial^2}{\partial a^2} U(a).$$

For the special contact repulsion $U(x) = c\delta(x)$, $c \rightarrow \infty$, imposed by the equivalence to the dimer model, the microscopic (short scale) c_{11} vanishes. However, on larger scales (or for more general microscopic interactions) c_{11} assumes a finite value due to entropic contributions. The resulting macroscopic c_{11} can be obtained from the free-energy density f of the model of Eq. (2) by¹⁸

$$c_{11} = a \frac{\partial^2}{\partial a^2} [af(a)]. \quad (8)$$

(BD). The continuum limit of the random SOS model is the RSG model with the reduced Hamiltonian⁸

$$H_{\text{RSG}} = \int d^2\mathbf{r} \left\{ \frac{K}{2} (\nabla h)^2 + \frac{V'}{T} \cos[Qh(\mathbf{r}) + \alpha(\mathbf{r})] \right\}, \quad (9)$$

where K is the reduced surface stiffness, $\alpha(\mathbf{r})$ is a spatially uncorrelated and uniformly distributed random phase, V' the coupling strength of disorder, and $Q = 2\pi/4$. The proper periodicity Q of the disorder coupling can be understood from the periodicity of the related discrete line lattice, i.e., via the path *ACED* in the diagram of Fig. 2. The latter sequence of mappings also allows to conclude about the value of the stiffness K in terms of the parameters of the discrete model, see below.

(ED). The two continuum models D and E differ by their form of elasticity (isotropic vs anisotropic) and the disorder coupling. If we set $h(\mathbf{r}) = 4u(\mathbf{r})/a$ and rescale the z axis in model E according to $z \rightarrow z' = z\sqrt{c_{11}/c_{44}}$ we obtain the isotropic elasticity of model D , cf. Eq. (9), with the stiffness given by

$$K = \frac{a^2 \sqrt{c_{11}c_{44}}}{16T}. \quad (10)$$

The disorder energy of Eq. (7) can be transformed to the form of Eq. (9) by expanding the local density of the lines $\rho(\mathbf{r})$ in terms of the line displacement $u(\mathbf{r})$ by use of Poisson's summation formula, for details see Ref. 2. The relation $h(\mathbf{r}) = 4u(\mathbf{r})/a$ between the line displacement field and the (dimensionless) height profile is the continuum version of Eq. (6) which can be seen with the use of Eq. (5) and the observation that $h_{ij}^{\text{ref}} \simeq 2j$ upon coarse graining. This relation is in hindsight, knowing that the lines have a mean distance of $a = 2b$, the reason for the choice of $Q = 2\pi/4$ in model D , Eq. (9). Due to the coordinate rescaling, the system size $A = L_x L_z$ is changed when going from model E to D . If we denote the system sizes by A_{el} and A_{RSG} , respectively, we obtain the ratio

$$\frac{A_{\text{RSG}}}{A_{\text{el}}} = \sqrt{\frac{c_{11}}{c_{44}}} = K \frac{8T}{bg}. \quad (11)$$

Having explained the relations between the models, we have to specify how the three continuum model parameters, (i) line stiffness $g = ac_{44}$, (ii) disorder strength Δ defined by Eq. (1), and (iii) temperature T , are related to the dimer model. First, we observe that only the relative strength of the parameters g and Δ with respect to thermal fluctuations is important, i.e., the ratios g/T and Δ/T^2 have to be determined. Out of these we start with the reduced single-line stiffness g/T . In the dimer model, out of the $2L^2$ bonds on average likewise $L^2/4$ horizontal and vertical bonds are occupied. This holds both with respect to thermal sampling, i.e., summing over dimer configurations, and the disorder average as long as the mean random energy is isotropic. For the discrete lines after the ‘‘XOR’’ addition with the reference state, an average number of $L^2/4$ horizontal and $L^2/2$ vertical segments is implied, corresponding to a mean line density of $\rho = 1/(2b)$. We now consider a given discrete line as performing a one-dimensional random walk with the three possibilities of moving to the left or to the right, or to rest. The probabilities for the possible steps $x_i = -1, 0, 1$ can be deduced from the average number of occupied horizontal and vertical bonds. From the above analysis of occupied bonds we find the corresponding probabilities $w_i = 1/4, 1/2, 1/4$ for the steps x_i . For the fluctuations of the total horizontal wandering $X \equiv \sum_i x_i$ this leads after z/b steps to

$$\langle X^2 \rangle = \sum_{i=1}^{z/b} \langle x_i^2 \rangle = zb/2.$$

TABLE I. Relation between parameters of the continuum line lattice and the dimer model with random vertical *and* horizontal bond energies (isotropic) or only random vertical bond energies (anisotropic).

Model	Line density	Line tension	Disorder	System size
Continuum line lattice	$\rho \equiv 1/a$	g/T	Δ/T^2	$L_x \times L_z$
Isotropic dimer model	$1/(2b)$	$2/b$	$\approx 2\xi_d/(bT_d^2)$	$bL \times \frac{16KT}{ag} - bL$
Anisotropic dimer model	$1/(2b)$	$2/b$	$\approx \xi_d/(bT_d^2)$	$bL \times \frac{16KT}{ag} - bL$

A continuum Hamiltonian for a random walk $H = (g/2) \int dz (\partial_z X)^2$ in comparison yields $\langle X^2 \rangle = (T/g)z$ and allows to read off

$$\frac{gb}{T} = 2. \quad (12)$$

The strength of disorder is measured in the continuum theory by the variance Δ of the disorder potential. Noting that $1/T_d^2$ is the variance of the (reduced) random bond energies in the dimer model we are led to identify $\sqrt{\Delta}/T$ with the dimensionless inverse dimer temperature $1/T_d$. Allowing for the finite disorder correlation length ξ_d , cf. Eq. (1), which acts as a cutoff in the continuum model, to differ slightly from the lattice constant b of the dimer model, we have

$$\frac{\Delta}{T^2} = \frac{\xi_d}{b} \frac{1}{T_d^2}. \quad (13)$$

A closer look at the models, however, suggests that this relation is valid only if the energies ϵ_{ij} of the horizontal bonds of the dimer model are set to zero, i.e., if there is no disorder on these bonds. This is because in the continuum model of Eq. (7) the disorder energy is written as the coupling of the local line density $\rho(\mathbf{r})$ to the disorder potential $V(\mathbf{r})$,

$$H_{\text{dis}} = \int dx dz V(x, z) \rho(x, z) = \sum_i \int dz V(x_i(z), z).$$

The random part of the energy is thus not an integral over the arc length of the lines but over their z coordinate. Therefore, the disorder energy of a line is proportional to its length projected onto the z axis and not to its overall length. In the original isotropic dimer model, random energy is collected on both vertical and horizontal bonds and will thus be proportional to the overall length of a fluctuating line. As a consequence, a given disorder in the dimer model corresponds to larger disorder in the continuum line model than assumed by Eq. (13). A possible method to gauge the disorder strength is to consider the annealed disorder average $-T \ln \bar{Z}$ of the free energy. This quantity can be obtained analytically in both models. The calculation for the continuum model is straightforward whereas in the dimer model the means of Ref. 16 together with the relation of Eq. (4) can be used. One finds by comparison between the two models the relation

$$\frac{\Delta}{T^2} = \frac{\xi_d}{b} \frac{2}{T_d^2} \left\{ 1 - \frac{2GT_d^2}{\pi} + \frac{2T_d^2}{\pi} \int_0^{e^{-1/(2T_d^2)}} dx \frac{\arctan x}{x} \right\} \quad (14)$$

with Catalan's constant $G = 0.915966$. The contribution from the latter two terms in the curly brackets crosses over at $T_d \approx 1$ from zero at small T_d to $-1/4$ at large T_d . Thus the overall factor of 2 as compared to the naive estimate of Eq. (13) confirms the conjecture about the contribution of the horizontal random bond energies for strong disorder (small T_d). For weak disorder (large T_d) the gauging by the annealed free energy yields a factor of $3/2$ compared to Eq. (13). However, in most expressions below, the latter two terms will only act as corrections at intermediate $T_d \approx 1$ and are in those cases frequently neglected. (At large T_d constant additional terms which are not related to the gauging procedure dominate.) It should be noted that the exact relation, Eq. (14), has been derived for one special observable, the annealed free energy, and it cannot be expected to hold universally for all observables with the same value for the regularization length ξ_d . Rather, to different observables the short-scale modes around the UV cutoff can contribute with a different weight. The one free parameter ξ_d/b relating the continuum model to the discrete model will therefore be considered a fitting parameter, which should, however, not turn out to vary dramatically around its expected value of order unity from observable to observable.

Below, results from numerical simulations of both the isotropic dimer model with random energies on vertical and horizontal bonds and the dimer model with vanishing energies on the horizontal bonds will be compared to theory. For the former, Eq. (14) will be used as disorder strength mapping (sometimes without the correction terms) while for the latter Eq. (13) will prove to fit very well. Table I summarizes the relations between the dimer parameters and the continuum model parameters.

III. REPLICA BETHE ANSATZ

The classical statistics of fluctuating elastic lines in d dimensions can be described by the quantum statistics of a $(d-1)$ -dimensional system of interacting bosons.¹⁹ In the thermodynamic limit, the free energy and its disorder fluctuations are determined by the ground-state energy of the Bose gas. An important simplification arises for $(1+1)$ -dimensional systems of self-avoiding lines for two reasons. First, in the absence of quenched disorder the interacting Bose gas is replaced by a one-dimensional free Fermi

gas since the noncrossing condition for the lines is then automatically fulfilled by the Pauli exclusion principle.^{20,21} Second, one-dimensional quantum systems with sufficiently simple interactions (generated here by quenched disorder) can be often treated exactly by Bethe *Ansatz*. Indeed, Kardar used the replica method to show that the self-avoiding line lattice in a random potential maps to a gas of fermions with n spin components with $SU(n)$ symmetry interacting via an attractive δ -function potential.¹⁰ The ground-state energy of this system can be calculated exactly by Bethe *Ansatz*. The analogy between the replicated line lattice and $SU(n)$ fermions was examined further in Ref. 11. In the following we will summarize the main results of the RBA.

Upon replication of the system of Eq. (2) and disorder averaging with the aid of Eq. (1), the equivalent quantum system is described by the Hamiltonian

$$\hat{H} = -\frac{T^2}{2g} \sum_{\alpha=1}^n \sum_{j=1}^N \frac{\partial^2}{\partial x_{j,\alpha}^2} - \frac{\Delta}{T} \sum_{\alpha < \beta} \sum_{j,k} \delta(x_{j,\alpha} - x_{k,\beta}), \quad (15)$$

where N is the number of lines and n the number of replicas. In the quantum system the line stiffness g corresponds to the fermion mass, the temperature T is mapped onto \hbar , and the system size in z direction, L_z , onto $\hbar\beta$ where β is the inverse quantum temperature. We are interested in the ground state with $SU(n)$ symmetry and the corresponding energy $E_0(n)$. As a function of the replica index n , the ground-state energy E_0 carries information on the statistics (cumulants) of the line-lattice free energy. The disorder averaged moments of the line-lattice partition function are given by

$$\ln \bar{Z}^n = \sum_{j=1}^{\infty} \frac{(-n)^j}{j!} \frac{\bar{F}_c^j}{T^j} = -\frac{E_0(n)L_z}{T} + n \frac{L_x}{a} \ln Z_0. \quad (16)$$

Here, \bar{F}_c^j are the cumulants of the disorder distributed line-lattice free energy and Z_0 is the partition function of a single line with no disorder contributions. The above expansion in the number of replicas n relies on the assumption of analyticity of the replica free energy (or ground-state energy) around $n=0$. That this assumption is indeed justified will be demonstrated below.

The model of Eq. (15) is integrable and its ground-state energy can be obtained in terms of n nested Bethe *Ansatz* as demonstrated by Sutherland²² for the repulsive case, and by Takahashi²³ and Kardar¹⁰ for the attractive case of interest here. For the Bethe *Ansatz* calculation n is assumed an integer number. In order to extract information from the ground-state energy about the thermodynamics of the line lattice, $E_0(n)$ has to be analytically continued to real valued n . $E_0(n)$ in the limit $n \rightarrow 0$ has been obtained in Ref. 10. Using a different method for the analytical continuation, an expression for $E_0(n)$ at arbitrary n was derived in Ref. 11. The result of the latter reference can be summarized as follows. The Bethe *Ansatz* equations can be analytically continued and thus yield the allowed wave numbers of the ground-state wave function for general n . The ground-state energy can then be expressed in terms of the density function $\varrho(k)$

which yields the number $L_x \varrho(k) dk$ of allowed wave numbers in the interval $[k, k+dk]$. One finds

$$E_0(n) = \frac{g\rho\Delta^2 L_x}{24T^4} n(1-n^2) + n \frac{T^2 L_x}{2g} \int_{-K}^K dk k^2 \varrho(k). \quad (17)$$

The (n -dependent) density function $\varrho(k)$ is determined by the integral equation

$$nk = \int_{-K}^K dk' g_n [(k-k')l_d] \varrho(k') \quad (18a)$$

with the kernel

$$g_n(x) = 2 \sum_{m=0}^{\infty} \arctan \left[\frac{nx}{m^2 + nm + x^2} \right]. \quad (18b)$$

The length $l_d = T^3/(g\Delta)$ is the characteristic length scale of the interaction in the quantum problem. This length sets the crossover scale beyond which the line fluctuations are dominated by disorder. In the above equations, the integral boundary K is fixed by the mean line density via

$$\rho = \int_{-K}^K dk \varrho(k). \quad (18c)$$

In the limit $n \rightarrow 0$, the integral equation (18a) assumes the form^{10,11}

$$\int_{-K}^K dk' \left\{ \frac{1}{l_d(k-k')} + \pi \coth[\pi l_d(k-k')] \right\} \varrho(k') = k. \quad (19)$$

This equation can be solved perturbatively in Kl_d , yielding

$$\varrho(k) = \sqrt{1-(k/K)^2} \left[\frac{1}{2\pi} Kl_d - \frac{\pi}{24} (Kl_d)^3 + \frac{\pi^3}{144} \left(1 + \frac{2}{5} (kl_d)^2 \right) (Kl_d)^5 + \dots \right]. \quad (20)$$

In the opposite limit of vanishing disorder or $l_d \rightarrow \infty$, the exact solution is $\varrho(k) = 1/(2\pi)$. Using Eqs. (17) and (18c) the ground-state energy can be calculated from Eq. (20) perturbatively in Kl_d . Interestingly, it can be shown order by order in Kl_d that the *exact* result for the ground-state energy is obtained from the first two terms in the square brackets of Eq. (20). Indeed one finds that¹³

$$\int_{-K}^K dk k^2 \varrho(k) = \frac{\pi^2}{3} \rho^3 + \rho^2 l_d^{-1} \quad (21)$$

to any order in ρl_d . Using $\bar{f} = \lim_{n \rightarrow 0} E_0(n)/(nL_x)$ this leads to the mean free energy density of the line system,

$$\bar{f} = \bar{f}_0 \rho + \frac{\pi^2}{6} \frac{T^2}{g} \rho^3 + \frac{\Delta}{2T} \rho^2, \quad (22)$$

where the contribution from single noninteracting lines is given by

$$\bar{f}_0 = C(g)T - \frac{\Delta}{2\xi_d T} + \frac{g\Delta^2}{24T^4}, \quad (23)$$

with $C(g)$ a disorder-independent contribution that cannot be obtained from Bethe *Ansatz*. The result for interacting lines [Eq. (22)] was first derived in Ref. 13 while the latter result for a single line was first given in Refs. [10,24]. In the latter works the $n \rightarrow 0$ limit was taken after the thermodynamic limit which results for a *single* line (or directed polymer) in vanishing second, fourth, and higher free-energy cumulants which was found to be not consistent with numerical results²⁵ and motivated further research for this problem.²⁶ However, very recent work by Brunet and Derrida²⁷ gave strong evidence for the applicability of the replica Bethe *Ansatz* even for finite-size systems where it yields finite second- and fourth-order free-energy cumulants. For the present system with a finite density of lines we will see below that all free-energy cumulants are finite and scale linear with the system size. It should be noted that in the interaction energy of Eq. (22) the entropic thermal contribution—second term—and steric disorder contribution—third term—are simply additive with no interference between the two effects. They agree in their dependency on the system parameters with the respective expressions based on scaling arguments.^{20,24}

So far we have only used the integral equation (18a) in the limit $n \rightarrow 0$. However, this equation taken at small n contains information about the cumulants of the free energy. Therefore, we would like to compute the ground-state energy $E_0(n)$ perturbatively in $n \ll 1$. In general, this is not feasible by analytical means. Therefore, below we will solve Eq. (18a) numerically in order to extract the behavior of E_0 for small n . There is, however, one important limiting case where analytical progress is possible. For strong disorder or low line density with $l_d \ll 1/\rho$, the integral, Eq. (18a), has been shown to assume a particular interesting form. It reduces¹¹ after a rescaling to the Bethe *Ansatz* equation for the one-dimensional Bose gas with a *repulsive* δ -function interaction.²⁸ The effective interaction strength of the Bose gas is proportional to n^2/l_d . Therefore, in the interesting limit of small n one can either use the numerical solution of the Bethe *Ansatz* equations for the Bose gas¹¹ or Bogoliubov's perturbation theory²⁹ to calculate the ground-state energy $E_0(n)$ of the SU(n) fermions as a polynomial in n to lowest order in ρl_d . From $E_0(n)$ the quenched averaged moments of the partition function of the line system can be evaluated using Eq. (16). For the disorder-dependent contributions one finds the result¹¹

$$\begin{aligned} \ln \bar{Z}^n = & -\frac{L_x L_z}{2} \left(\frac{\Delta}{T^2} \right)^3 \left(\frac{g}{T} \right)^2 \left\{ \frac{n}{12} (1-n^2) l_d \rho + n (l_d \rho)^2 \right. \\ & \left. - \frac{4}{3\pi} n^2 (l_d \rho)^{3/2} + \left(\frac{1}{6} - \frac{1}{\pi^2} \right) n^3 l_d \rho + O(n^4) \right\}. \end{aligned} \quad (24)$$

The first term $\sim (1-n^2)\rho$ in the curly brackets describes the disorder contribution to the single-line free-energy cumulants

while the following terms stem from line interactions in the presence of disorder. As can be seen from Eq. (16) the above result provides the free-energy cumulants in the dilute limit $\rho l_d \ll 1$. At higher densities, the mapping to the Bose gas is no longer valid and the ground-state energy has to be calculated by direct numerical solution of the integral, Eq. (18a). This will be done in Sec. IV C.

A natural limit to the validity of the RBA results is set by the mapping of the line system with short-ranged correlated disorder to the quantum problem with a singular δ -function interaction arising from the disorder average. The characteristic length scale in the quantum problem is l_d which is inversely proportional to the disorder strength Δ . If l_d becomes of the order of the cutoff length ξ_d of the short-ranged disorder correlator of Eq. (1), the assumption of ultralocally interacting fermions is no longer justified. The δ -function interaction, however, is essential for the Fermi gas to be solvable by Bethe *Ansatz*. The RBA results therefore are valid only for temperatures

$$T \geq T^* = (g \xi_d \Delta)^{1/3}, \quad (25)$$

or, respectively, at sufficiently weak disorder. For lower temperatures a modified replica symmetry-breaking solution has been suggested in Ref. 30 for the single line, the predictions of which, however, could not be tested to date by other means. For the interacting line system the modifications at low temperatures implied by the replica symmetry-breaking solution can be adapted.¹¹ However, when the RBA results are translated to the random bond dimer model it turns out that the low-temperature limit $T < T^*$ can be never realized in the latter model.

IV. THERMODYNAMICS

A. Large-scale equivalence

Before studying thermodynamics, we will demonstrate that the statistics of the random bond dimer model and its associated discrete height profile on large length scales are well described by the continuum model for elastic lines which can be treated analytically by the RBA. From the simulation of the random bond dimer model, the correlations of the height profile $\{h_{ij}\}$ of model *B* can be determined very accurately. The quantity $\delta h(\mathbf{r}) = h(\mathbf{r}) - \langle h(\mathbf{r}) \rangle$ measures the thermal fluctuations of the height around its state pinned by disorder. A renormalization-group calculation predicts for the disorder averaged correlation function²

$$C(\mathbf{r}) = \overline{\langle [\delta h(\mathbf{r}) - \delta h(\mathbf{0})]^2 \rangle} = \frac{1}{\pi K} \ln(|\mathbf{r}|/b), \quad (26)$$

i.e., logarithmic growth on large scales, irrespective of the value of $\langle h(\mathbf{0}) \rangle$. A possible transition from a glassy low-temperature phase with $\langle h(\mathbf{0}) \rangle > 0$ to a free thermal phase with $\langle h(\mathbf{0}) \rangle = 0$ therefore is not reflected directly in this correlation function. However, the coefficient $1/(\pi K)$ will be of interest. The stiffness K obtained from a measurement of the correlation function for large $|\mathbf{r}|$ is the *large-scale* effective stiffness, renormalized by contributions from thermal and disorder fluctuations on smaller scales. It can be calculated

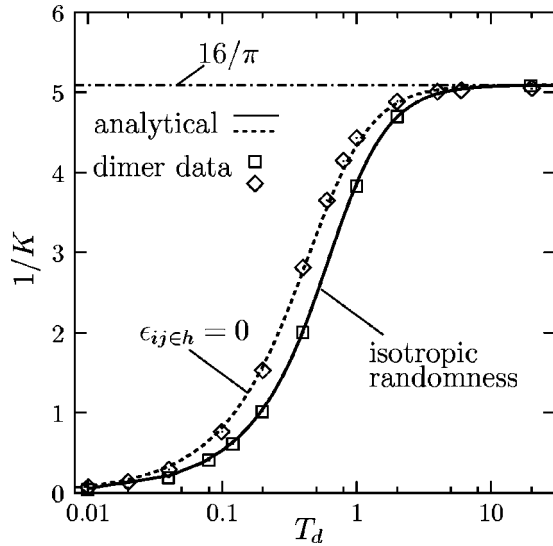


FIG. 5. Large-scale stiffness K as a function of the inverse disorder strength T_d . Shown are the simulation results for the dimer model with isotropic random energies and for the model with random energies only on the vertical bonds together with the RBA result of Eq. (27). In the isotropic case T_d and Δ are related by Eq. (14) with $\xi_d = 1.15$ while in the anisotropic case Eq. (13) with $\xi_d = 0.83$ has been used.

exactly from the RBA free energy, Eq. (22). First one can use the thermodynamic definition of the compression modulus of Eq. (8),

$$c_{11} = a \partial_a^2 [a f(a)],$$

and then gets via the relation of Eq. (10) the effective stiffness

$$K = \frac{\pi}{16} \left(1 + \frac{ag\Delta}{\pi^2 T^3} \right)^{1/2}. \quad (27)$$

Note that due to its linear dependence on density, the single-line free energy of Eq. (22) does not contribute to K . The result of Eq. (27) is compared in Fig. 5 to the numerical result as obtained from the dimer model with isotropic disorder (see also Ref. 8) and from the dimer model with no random energies on the horizontal bonds, i.e., $\epsilon_{ij \in h} = 0$. The disorder strength Δ has been mapped here to T_d according to Eq. (14) and Eq. (13), respectively. The agreement is very good over orders of magnitude while the Δ - T_d relation from the comparison of annealed free-energy averages seems to fit better than the naive estimate. The validity of the replica Bethe *Ansatz* calculation including its sometimes debated analytical continuation in n is nicely confirmed by our comparison. Interestingly, no deviation from the RBA result of Eq. (27) is found in the large disorder, i.e., low- T_d limit. In terms of the line-lattice temperature T modifications of the result of Eq. (22) must occur at $T \leq T^*$, cf. Eq. (25), since otherwise the free energy would not converge to a finite ground-state energy for $T \rightarrow 0$. However, this problem no longer exists after the mapping to the dimer model since the ratio $\sqrt{\Delta}/T$ of disorder and thermal energy is controlled by

the single parameter T_d^{-1} in the dimer model. Thus the pinning strength and thermal fluctuations cannot be varied independently, and the crossover temperature T^* can vanish.

In the pure limit $T_d \rightarrow \infty$ the stiffness approaches the value $K = \pi/16$ in agreement with both the exact calculation in terms of the nonrandom dimer model¹⁷ and the mapping of the line lattice without disorder to free fermions. Hence the most accurate simulation of a system of noncrossing lines by the dimer model is demonstrated. The precise value $K = \pi/16$ is of physical significance as shown by the RG scaling dimension of disorder in RSG model Eq. (9),

$$\lambda_\Delta = 2(1 - \pi/16K^{-1}), \quad (28)$$

see also Ref. 13. The limiting value of $K = \pi/16$ indicates that infinitesimal disorder is marginal and the system is thus on the borderline between a glassy and a thermal free phase. Any finite amount of disorder increases K which in turn renders disorder a relevant perturbation, leading to a glassy phase. This is consistent with the finding of Ref. 8 that the correlation function of the height profile, i.e., the one of h and not of δh , always indicates a low-temperature glassy behavior.

B. Free energy, internal energy, and entropy

We now come to a direct comparison of fundamental thermodynamic quantities of the dimer model and of the continuum model for the line lattice. We start with the disorder averaged free energies $\bar{F} = -T \overline{\ln Z}$. Due to the different meanings of temperature in the line and dimer context we will focus on the logarithm of the partition functions $\overline{\ln Z}$. When relating the systems we remember the energy relation, Eq. (4), between dimer and line configurations. Therefore, the partition functions Z_d of the dimer model and Z_l of the line lattice are related by

$$\ln Z_d + E_{\text{ref}}/T_d = \ln Z_l. \quad (29)$$

In the disorder average $\overline{\ln Z_d + E_{\text{ref}}/T_d}$ the reference energy $E_{\text{ref}} = H_{\text{ref}}(\{\epsilon'_{ij}\})$, cf. Eq. (4), does not contribute as the bond energies are drawn from a Gaussian distribution with zero mean. Higher moments of the free energy, however, contain contributions from E_{ref} . In the simulations of the dimer model the moments of the density $\ln(Z_l)/(bL)^2$ are measured by taking into account the reference energy E_{ref} . The RBA, however, provides the statistics of the free-energy density of the line lattice [Eq. (22)] which we denote by f_l in the following. Both quantities are related by

$$\frac{\ln Z_l}{(bL)^2} = -\frac{A_l f_l}{A_d T}, \quad (30)$$

where $A_l = L_x L_z$ and $A_d = (bL)^2$ are the system sizes of the line lattice and dimer model, respectively. Here we have to pay attention to the fact that the two models are only equivalent after a rescaling of the z coordinate as explained for the mapping between the models *D* and *E* in Sec. II C. According to Eq. (11) we have

$$\frac{A_l}{A_d} = \frac{a}{16K} \frac{g}{T} = \frac{a}{\pi} \frac{g}{T} \left(1 + \frac{ag\Delta}{\pi^2 T^3} \right)^{-1/2}$$

which has to be used in Eq. (30). The disorder-independent part of the single-line mean free energy \bar{f}_0 cannot be calculated unambiguously by the RBA. We thus combine the disorder-independent contributions in \bar{f}_l such that in the pure limit ($T_d \rightarrow \infty$) the known free energy of the dimer model is matched. In this limit, the partition functions of the dimer model just count the number of complete dimer coverings of the square lattice. This is a complex combinatorial problem as any flip of one dimer may necessitate a cascade of flips throughout the system. Nevertheless, the result is exactly known to be¹⁶

$$\ln Z_d|_{T_d \rightarrow \infty} = \frac{G}{\pi} L^2 \quad (31)$$

in the thermodynamic limit with Catalan's constant $G = 0.915966$. Next, we translate the line-lattice parameters to the dimer model along Table I and get for the dimer model without horizontal energies ($\epsilon_{ij \in h} = 0$)

$$\frac{\ln Z_l}{L^2} = \frac{1}{\sqrt{\pi^2 + 4\xi_d/(bT_d^2)}} \left[G + \frac{1}{T_d^2} \left(1 - \frac{\xi_d}{2b} \right) - \frac{1}{6} \frac{\xi_d^2}{b^2 T_d^4} \right]. \quad (32)$$

If both vertical and horizontal bonds carry random energies one should make the approximate replacement $1/T_d^2 \rightarrow 2/T_d^2$, which can be improved by the correction terms of Eq. (14), as explained above. The second term $\sim T_d^{-2}$ in the square brackets of Eq. (32) comes from terms proportional to disorder in both the single-line free energy and the interaction part. The last term $\sim T_d^{-4}$ comes from the term $\sim \Delta^2$ in the single-line free energy. When comparing the result of Eq. (32) to the simulation results for the dimer model, at first glance we find no agreement at all. However, as we will discuss shortly, there are indications that one might have to drop the T_d^{-4} term of Eq. (32). Doing so, we get the plots of Fig. 6 for the isotropic and the anisotropic random bond energies. Only the large T_d limit was fixed by the known result of Eq. (31), yet the agreement is excellent over orders of magnitude down to small dimer temperatures. The only fitting parameter ξ_d/b arising from the disorder strength relation between the discrete and the continuum model is found, as expected, to be of order 1, cf. the caption of Fig. 6.

Why do we have to drop the Δ^2 term of the single-line free energy [Eq. (23)] to obtain agreement? One can, in fact, imagine a number of reasons for this discrepancy between the RBA result and the simulation data. The validity of the RBA itself has been critically discussed, especially the interchange of thermodynamic limit and replica number $n \rightarrow 0$ limit has been questioned. On the other hand, the simulations are performed for discrete lattice versions of the continuum model which has been solved by RBA. We were not able to find a conclusive answer to what causes the absence of the Δ^2 term in the simulation data. But in connection to this it is interesting to remind of a numerical analysis of the average

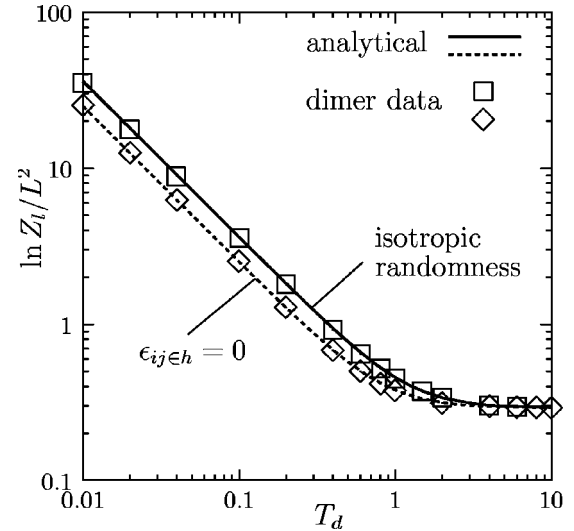


FIG. 6. Comparison of the disorder averaged free energy as obtained from the dimer model simulations and Eq. (32), respectively. $\ln Z_l/L^2$ is plotted against dimer temperature $T_d \sim T/\sqrt{\Delta}$ for the isotropic dimer model ($\xi_d/b = 0.96$) and the one with random energies only on the vertical bonds ($\xi_d/b = 1.00$). The simulation data are for system size $L \times L = 256 \times 256$.

free energy of a single directed polymer in a random potential via a transfer-matrix method in Ref. 31. In Fig. 7 the simulation data of Table II of Ref. 31 are plotted, giving the average free energy as a function of disorder strength. A plot of this kind had not been shown in the cited reference. However, it demonstrates that the data obtained in Ref. 31 agree with ours in *not* finding support for the term $\sim \Delta^2$ in Eq. (23).

Now we compare further thermodynamic quantities for the dimer model and the line lattice. The entropy and the internal energy of the dimer model

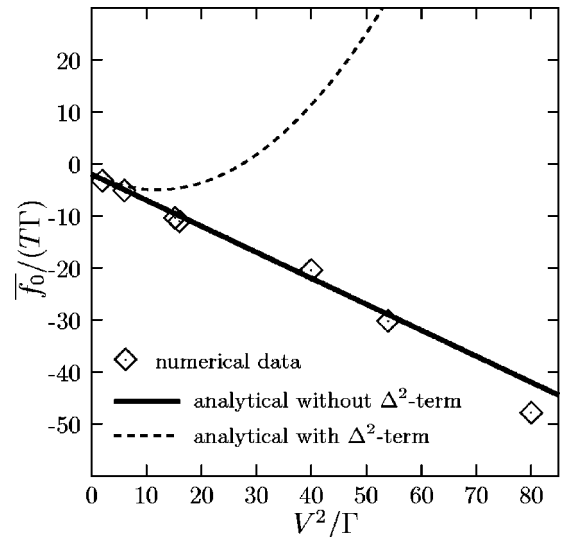


FIG. 7. Single-line average free energy \bar{f}_0 plotted against disorder strength $V^2 \sim \Delta$; data taken from Table II of Ref. 31, $\Gamma \sim 1/g$. The solid and dashed curves show the analytical result of Eq. (23) without and with the term $\sim \Delta^2$, respectively. The reason for the discrepancy is discussed in the text.

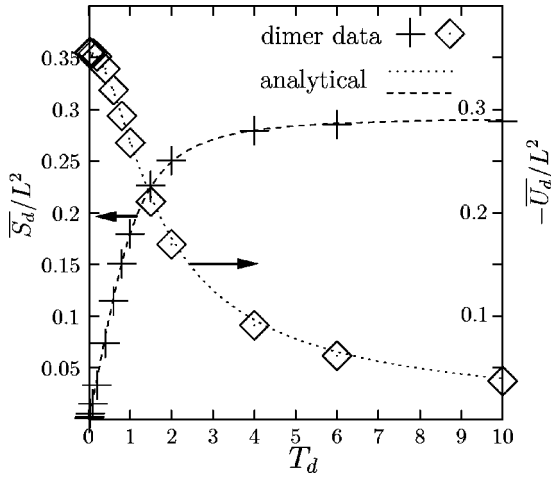


FIG. 8. Comparison between simulation data and RBA result for the quenched average entropy density \bar{S}_d/L^2 ($\xi_d/b=0.98$) and internal energy density \bar{U}_d/L^2 ($\xi_d/b=1.00$). The data are for system size $L=256$.

$$\bar{S}_d = -\frac{\partial}{\partial T_d} \bar{F}_d = \frac{\partial}{\partial T_d} (T_d \overline{\ln Z_d}),$$

$$\bar{U}_d = \bar{F}_d + T_d \bar{S}_d$$

are easily calculated from the RBA. In the dimer model simulations, the quenched averaged internal energy $\bar{U}_d = \overline{\sum_{(ij)} p(ij) \epsilon_{ij}}$ with the disorder configuration-dependent dimer occupation probability $p(ij)$ of bond (ij) can be obtained quite easily since the polynomial algorithm allows to calculate the probabilities $p(ij)$. The entropy is then obtained from the free energy by subtraction. A comparison of the data for internal energy and entropy with the RBA prediction is given in Fig. 8 where we used the result of Eq. (32) and $\ln Z_d = \ln Z_l$ to calculate \bar{S}_d and \bar{U}_d . We find excellent agreement with $\xi_d/b \approx 1$. The slope of \bar{S}_d at $T_d=0$ is calculated from Eq. (32) to be

$$\frac{1}{L^2} \frac{\partial}{\partial T_d} \bar{S}_d |_{T_d=0} = G \left(\frac{b}{\xi_d} \right)^{1/2} - \frac{\pi^2}{8} \left(\frac{b}{\xi_d} \right)^{3/2} \left(1 - \frac{\xi_d}{2b} \right) \quad (33)$$

and matches the simulation data very well.

Summarizing, the quantitative agreement between the RBA results for the line lattice and simulation data for the dimer model is very satisfying; it is even more surprising for the thermodynamic potentials than for the large-scale stiffness. The latter is expected to show universality in the sense that it does not depend on microscopic details of the model, while the former receive contributions from all scales. *A priori*, the sensitivity to the contribution from modes close to the UV cutoff might have been expected to be important. However, our above results indicate that the effect of small scales can be simply accounted for by the single-fit parameter ξ_d/b which was found to be very close to the naively expected value of 1.

C. Higher moments

Higher cumulants of thermodynamic quantities describe sample-to-sample fluctuations in experimental setups of mesoscopic dimensions while for macroscopic systems their scaling will give information on the self-averaging behavior. Analytic expressions for higher cumulants of the free energy are available¹¹ only in the strong disorder or dilute limit $l_d \rho \ll 1$, see Eq. (24). At higher densities we have to resort to a numerical computation of the ground-state energy which then yields $\ln \bar{Z}^n$ via Eq. (16), and thus the cumulants of the free energy. In the following we are interested in a polynomial expression for $E_0(n)$. Thus we have to expand in Eq. (17) the integral of the kinetic energy with respect to n . We introduce the dimensionless integral

$$\begin{aligned} \tilde{E}_{\text{kin}}(n) &\equiv b^3 \int_{-K}^K dk k^2 \varrho(k) \\ &= (bK)^3 \int_{-1}^1 dy y^2 \tilde{\varrho}(y) \equiv \sum_{j \geq 0} \epsilon_{j+1} (\rho l_d) n^j, \end{aligned} \quad (34)$$

defining the expansion coefficients $\epsilon_j(\rho l_d)$ which depend only on the dimensionless parameter ρl_d . With this definition, explicit formulas for the variance (second cumulant) and the skewness (third cumulant) of the reduced free energy can be obtained from the RBA. Using Eqs. (16) and (17) together with Eq. (34) and the perturbative result of Eq. (24) we get

$$\frac{\overline{(\ln Z_l)_c^2}}{L^2} = \begin{cases} -\frac{A_l}{A_d} \frac{T b^2}{g} \epsilon_2(\rho l_d) & \rightarrow -\frac{A_l}{A_d} \frac{1}{2} \epsilon_2(T_d) \quad (\text{exact RBA}) \\ \frac{A_l}{A_d} \frac{4}{3\pi} \left(\frac{b\Delta}{aT^2} \right)^{3/2} \left(\frac{bg}{T} \right)^{1/2} & \rightarrow \frac{A_l}{A_d} \frac{2}{3\pi} \frac{(\xi_d/b)^{3/2}}{T_d^3} \quad (\text{perturbative, } T_d \ll 1), \end{cases} \quad (35)$$

$$\frac{\overline{(\ln Z_l)_c^3}}{L^2} = \begin{cases} \left\{ \frac{A_l}{A_d} \left[\left(\frac{\Delta}{T^2} \right)^2 \frac{bg}{T} \frac{b}{4a} - \frac{3Tb^2}{g} \epsilon_3(\rho l_d) \right] \right\} & \rightarrow \frac{A_l}{A_d} \left\{ \frac{1}{4} \frac{(\xi_d/b)^2}{T_d^4} - \frac{3}{2} \epsilon_3(T_d) \right\} \quad (\text{exact RBA}) \\ \frac{A_l}{A_d} \left(\frac{3}{\pi^2} - \frac{1}{4} \right) \left(\frac{\Delta}{T^2} \right)^2 \frac{bg}{T} \frac{b}{a} & \rightarrow \frac{A_l}{A_d} \left(\frac{3}{\pi^2} - \frac{1}{4} \right) \frac{(\xi_d/b)^2}{T_d^4} \quad (\text{perturbative, } T_d \ll 1). \end{cases} \quad (36)$$

Here, the mapping $gb/T \rightarrow 2$, $\Delta/T^2 \rightarrow (\xi_d/b)/T_d^2$, $a \rightarrow 2b$, $\rho l_d \rightarrow (b/\xi_d)T_d^2/4$ between the line lattice and the dimer model with random energies only on the vertical bonds has been applied. Also the rescaling of the volume according to Eq. (11) has to be applied for the comparison. In terms of the dimer temperature T_d , the rescaling factor reads

$$\frac{A_l}{A_d} = \frac{ag}{\pi T} \left(1 + \frac{ag\Delta}{\pi^2 T^3} \right)^{-1/2} \rightarrow \frac{4}{\pi} \left(1 + \frac{4\xi_d/b}{\pi^2 T_d^2} \right)^{-1/2}.$$

In order to compare the above RBA results to simulation data for the dimer model over the whole range of disorder strength, we solve Eqs. (18a) and (18c) for $\rho(k)$ numerically. From $\rho(k)$ the kinetic energy of Eq. (34) and thus the expansion coefficients ε_j are obtained. For a numerical treatment it is useful to rewrite Eq. (18a) in the form

$$y = \frac{1}{n} \int_{-1}^1 dy' g_n [Kl_d(y-y')] \tilde{\varrho}(y') \quad (37)$$

with $y = k/K$ and $\tilde{\varrho}(y) = \varrho(Ky)$. At fixed Kl_d , the dimensionless function $\tilde{\varrho}(y)$ is computed by the inversion of the discretized integral equation. This inversion is quite delicate since the present kind of inverse problem—a Fredholm integral equation of the first kind—is extremely badly conditioned. An adequate treatment is, however, possible by use of, e.g., the method of singular-value decomposition of the discretized integral kernel.³² The solution $\tilde{\varrho}(y)$ can only be computed for a given value of Kl_d . With the so obtained solution we can calculate the right-hand side of

$$\frac{\rho}{K} = \int_{-1}^1 dy \tilde{\varrho}(y).$$

The dimer model density $\rho = 1/(2b)$ then fixes K and we thus obtain the disorder strength $1/l_d$ that had been implied by our initially chosen value for Kl_d . In this approach we cannot—due to the coupling of the BA equations—modify n and l_d independently. A modified n implies a modified K , which results in a different value of l_d . We hence have to adjust the parameter Kl_d in Eq. (37) upon change of n such that l_d remains constant. In practice, this is realized by the simple method of nested intervals. The necessary number of discretization points for the integral, Eq. (37), depends crucially on considered range of parameters. An increase in the length scale l_d stretches the integral kernel $g_n(kl_d)/n$ along the abscissa, a decreasing n does so along the ordinate. Thus, in order to keep up a given level of accuracy, the number of discretization points has to increase like l_d/n . We are unfortunately interested in small n as we want to extract the coefficients ε_j from the behavior around $n=0$ and moreover in large l_d as the result for small l_d is known analytically. Therefore it is important that the reliability of the numerics can be checked in limiting cases where analytical results for $\varrho(k)$ are available. The limit of large $l_d \rightarrow \infty$ or $n \rightarrow 1$ corresponds to lines without quenched disorder which are described by free fermions with a constant density $\varrho(k) = 1/(2\pi)$. In the inset of Fig. 9, a plot of the numerical

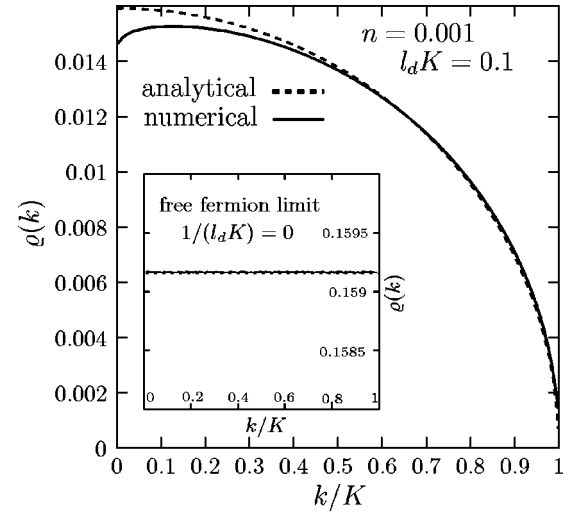


FIG. 9. Numerical solution $\varrho(k/K)$ for small $l_d K$, $n=0$ and for $l_d K \rightarrow \infty$ (inset). The mismatch at small k/K between the analytical expression and the numerical solution for $l_d K=0.1$ is reduced with an increasing number of discretization points. For the extraction of cumulants, larger values of n/l_d have been used where a discretization level of 10^3 points suffices.

solution in the latter case is displayed, showing very good agreement with the analytical expectation. Another limit which can be compared to analytical results corresponds to $n \rightarrow 0$. Then $\varrho(k)$ can be calculated perturbatively¹¹ in Kl_d , see Eq. (20). We compare the numerical solution for $n = 10^{-3}$ and $Kl_d=0.1$ with the result of Eq. (20) in Fig. 9. Again the comparison is satisfactory while the mismatch at small k/K is due to the smallness of n which necessitates a high discretization level. In practice, n is chosen as not to require more than 10^3 discretization points for a relative accuracy of 10^{-4} in $\tilde{E}_{\text{kin}}(n)$. Checks against the exact results for the quenched averaged free energy [Eq. (22)] and the strong disorder limit of the cumulants [Eq. (24)] are also satisfactory.

Having determined the solution $\rho(k)$, the coefficients ε_j of Eq. (34) can be extracted from the numerically calculated $\tilde{E}_{\text{kin}}(n)$ by repeated extrapolation to $n=0$, subsequent subtraction of this value from the finite- n result and final division by n . This straightforward procedure is the best we could think of but it is still error prone. While the desire for a small extrapolation error requires having data points as close as possible to $n=0$, a simple calculation of error propagation shows that the error of a given data point at finite n scales as $n^{-k} \delta \tilde{E}_{\text{kin}}$ where k stands for the order of the coefficient and $\delta \tilde{E}_{\text{kin}}$ for the original error of the data. However, we were able to achieve sufficient high accuracy to extract reliable values for the second and the third cumulant. The above described scheme was implemented with the use of numerical recipe routines.³² The data for the smallest disorder values needed the highest discretization level and consumed about 200 h computation time on a 2 GHz processor for the determination of the cumulants at a given value for l_d .

Before we compare the RBA predictions for the cumu-

lants to the simulation results for the dimer model we would like to make some remarks on the computation of cumulants in the dimer model simulations. In the replica theory the *cumulants* of random thermodynamic quantities appear naturally, while in the simulations the *moments* are immediately accessible. Both are related as follows. If the generating functional of the moments $\{m_p\}$ is

$$M(n) = 1 + nm_1 + n^2 \frac{m_2}{2!} + n^3 \frac{m_3}{3!} + \dots,$$

then

$$\ln M(n) = n\kappa_1 + n^2 \frac{\kappa_2}{2!} + n^3 \frac{\kappa_3}{3!} + \dots$$

generates the cumulants $\{\kappa_p\}$. The lowest cumulants expressed in terms of moments are

$$\begin{aligned} \kappa_1 &= m_1, & \kappa_2 &= m_2 - m_1^2, \\ \kappa_3 &= m_3 - 3m_1m_2 + 2m_1^3. \end{aligned} \quad (38)$$

From the dependence of Eq. (16) on the system size $A_l = L_x \times L_z$ it follows immediately that all the free-energy cumulants scale linearly in A_l . Apart from the average free energy, the reduced cumulants $\kappa_p/\kappa_1^p = \overline{F_c^p}/\overline{F}^p$ hence vanish in the thermodynamic limit as $\overline{F_c^p}/\overline{F}^p \sim A_l^{1-p}$ as one would expect from the central limit theorem. The distribution of the free energy becomes infinitely sharp in the limit of large systems. In other words, the vortex-line array is self-averaging which in light of the infinite correlation length reflected by logarithmic correlations had not been evident *a priori*.

For the determination of the cumulants from the simulation data the following problem is entailed. The moments m_p scale with the system size like $m_p \sim A_l^p$. From Eq. (38) we see that a cumulant of order p has to be calculated as a sum of terms that grow by a factor A_l^{p-1} faster with the system size than the cumulant itself. Therefore, at a given accuracy of the simulation data for the m_p , which primarily depends upon the number of disorder samples, a limit is set to the system size up to where cumulants can reliably be obtained. This maximum system size decreases with the order of the cumulant. On the other hand, finite-size effects have to be minimized as well and, as a consequence, at the achieved precision of 10^{-5} for the moments m_p in the dimer model, the variance can be trusted only for system up to size $L = 64$ and the third cumulant up to size $L = 16$.

In the following, we compare the simulation data for the cumulants $(\ln Z_l)_c^p/L^2$ for $p=2,3$ with the RBA predictions of Eqs. (35) and (36). The variance ($p=2$) as a function of T_d has been computed for the dimer model of size $L=64$ and is shown in Figs. 10 and 11 together with the RBA result. With the only fitting parameter $\xi_d/b=0.8$ we find very good agreement. In addition, the plots show that our numerical solution of the full Bethe Ansatz equations nicely confirms the perturbative solution at small T_d . The deviation at larger T_d shows that the numerical solution is inevitable for a com-

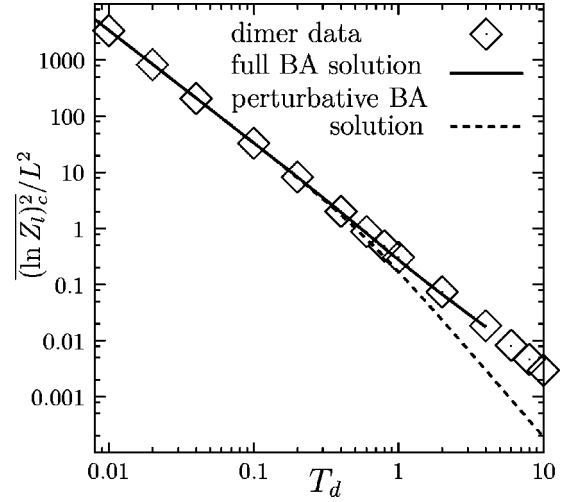


FIG. 10. Simulation data for the dimer model with random energies on the vertical bonds only (diamonds), the numerical result of the RBA equations (full line), and the perturbative RBA result (dashed line) for $(\ln Z_l)_c^2/L^2$. The fitting parameter is $\xi_d=0.8$, dimer system size is $L=64$.

parison with the simulation data. A closer look at the analytical result of Eq. (35) and the data points of Figs. 10 and 11 shows that $(\ln Z_l)_c^2/L^2$ does *not* follow strictly a power law in T_d . The third cumulant (skewness, $p=3$) is shown in Fig. 12. For the reasons explained above, the dimer data are to be trusted only for the small system $L=16$ and here only for $T_d \lesssim 1$. In this range, no substantial deviations from the perturbative evaluation of the cumulant, cf. Eq. (36), are expected. Indeed, the agreement between theory and simulation is again very good with $\xi_d/b=0.8$. Although the numerically determined coefficient ε_3 has an error of only $\sim 15\%$, the actual uncertainty of the third cumulant is larger. The reason is the following. In the exact RBA result of Eq. (36) the magnitude of the second term $\sim \varepsilon_3$ amounts throughout the studied parameter range to about 85% of the first term. Since the terms are subtracted, the original error of 15% gets

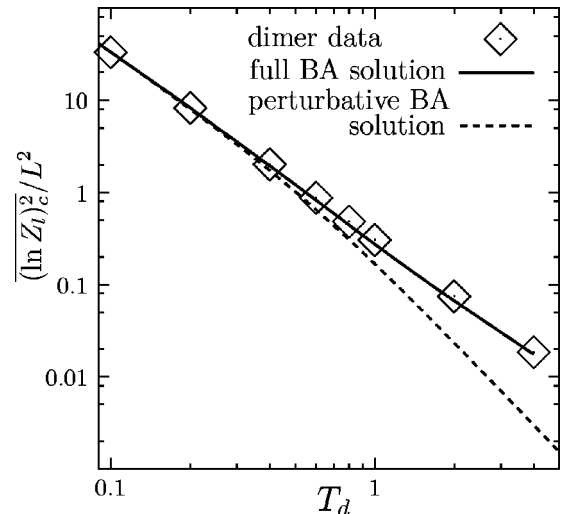


FIG. 11. Same as Fig. 10 with a smaller range of T_d .

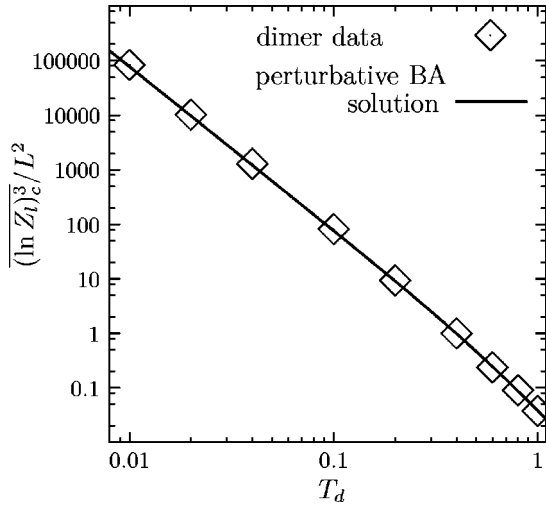


FIG. 12. Simulation data (diamonds) and perturbative RBA result (full line) for the third cumulant (skewness) $\overline{(\ln Z_l)_c^3}/L^2$. The dimer system size is $L=16$. Note that the data do not follow a power law.

amplified to $\sim 100\%$ in the final expression for the third cumulant. However, this does not restrict the comparison since the perturbative RBA solution could not have been corrected noticeably in the range $T_d \lesssim 1$ which is set by the simulation data at hand. Note that both the simulation data and the perturbative RBA result consistently do not obey a power law in T_d , see Fig. 12.

It must be noted that there is agreement for the third cumulant only if the term $\sim n^3$ from the single-line contribution $\sim (n/12)(1-n^2)\Delta^2$ in Eq. (24) is taken seriously, otherwise not even the sign of the cumulant would match. However, the part linear in n stemming from the same contribution we had to drop in the comparison of the average free energy, being consistent with another independent study³¹ of the single-line free energy. Since a single line (or

directed polymer) is expected to have an asymmetric disorder free-energy distribution, we do not argue for a complete irrelevance of the contributions $\sim \Delta^2$ in the single-line terms of Eq. (24), consistent with our simulation data for the third cumulant, but suggest a reassessment of the free-energy distribution of a single line in random media.

D. Specific heat

The specific heat of disordered systems is strongly influenced by the complex nature of thermal excitations about the pinned ground state. In the context of spin glasses the excitations are considered as droplets, i.e., connected regions in which the thermal activated configurations differ from the ground-state configuration.^{6,33} Droplets appear on all length scales with the lowest-energy ones appearing on largest length scales. Here we would like to test the RBA prediction for the mean specific heat by comparing to our simulation results. The disorder averaged specific heat of the dimer model with random energy on horizontal and vertical bonds can be measured via the thermal fluctuations of the dimer energy,

$$\overline{c_d} = L^{-2} \frac{\overline{\langle H_d^2 \rangle} - \langle H_d \rangle^2}{T_d^2}, \quad (39)$$

where H_d is the Hamiltonian of the dimer model, see Sec. II B. From the RBA result for the free energy, Eq. (22) (again without the Δ^2 term in the single-line free energy), the specific heat is calculated easily using

$$\overline{c_d} = \frac{T_d}{L^2} \frac{\partial^2}{\partial T_d^2} (T_d \overline{\ln Z_d}), \quad (40)$$

where $\overline{\ln Z_d} = \overline{\ln Z_l}$ is given by Eq. (30). After the mapping $\Delta/T^2 \rightarrow 2(\xi_d/b)/T_d^2$, $bg/T \rightarrow 2$, $\rho \rightarrow 1/(2b)$, the mean specific heat of the dimer model reads

$$\overline{c_d} = \frac{2\pi^2 [2\pi^2 - (\xi_d/b)(\pi^2 + 4G)] T_d^3 - 8 [2\pi^2 - (\xi_d/b)(\pi^2 + 16G)] (\xi_d/b) T_d}{[\pi^2 T_d^2 + 8(\xi_d/b)]^{5/2}}. \quad (41)$$

In Fig. 13 we compare this RBA result to the simulation data which we obtained via Eq. (39). We find rather nice agreement over the entire range of T_d with the choice $\xi_d/b = 0.98$ for the only fitting parameter, which is consistent with our findings above. There are no further adjustable parameters in the comparison shown in Fig. 13. Also note that the dimer specific heat probes for the agreement of the RBA and simulations predominantly in the region around $T_d \approx 1$, the drop to zero for small and large T_d being generic rather than specific. So it can be considered complementary to the mean free energy which tested for amplitude and exponent at small T_d while the large T_d (or pure) limit was fixed to the exactly known result, see Sec. IV B.

The linear low-temperature behavior of the specific heat is typical of random systems. It can easily be understood by considering the lowest-lying excitations on a given length scale ℓ . On each scale for a given disorder environment the ground state (with zero energy) and the lowest excitation (with energy E) form a two-level system, whose specific heat is

$$c_{\ell,E} = \frac{\partial}{\partial T} \frac{E e^{-E/T}}{e^{-E/T} + 1}.$$

The excitation energies obey a length scale dependent disorder distribution $p_\ell(E)$ and the contribution to the mean spe-

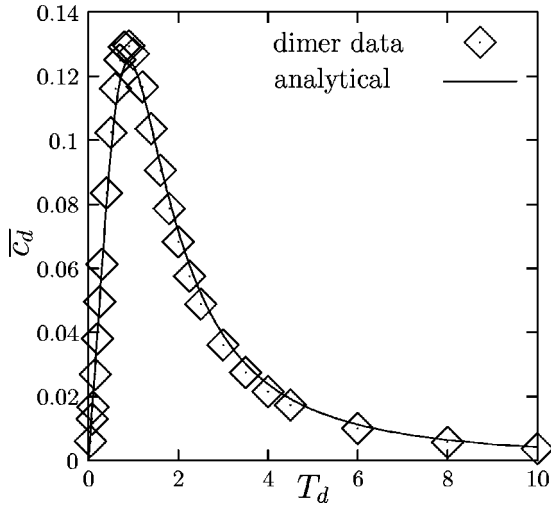


FIG. 13. Mean dimer specific heat \bar{c}_d . Shown are the simulation data (diamonds) and the analytical result of Eq. (41) derived from the RBA (full line). The simulated dimer model has random energies on horizontal and vertical bonds, and is of size $L=256$.

cific heat from each scale is

$$\delta\bar{c}_\ell = \int_0^\infty dE p_\ell(E) c_{\ell,E} \sim p_\ell(0+)T.$$

For a finite density of excitations at small energies, $\lim_{E \rightarrow 0} p_\ell(E) > 0$, the specific heat as a superposition of exponential contributions from each scale will be *linear* at small temperatures which is a famous insight of Anderson *et al.*³⁴ Integration over all length scales allows to write the mean specific heat as $\bar{c} = \int_0^L d\ell \delta\bar{c}_\ell$ which becomes exact in the limit $T \rightarrow 0$. In the droplet theory of spin glasses the distribution function $p_\ell(E)$ is a central quantity. From the finite-size scaling of the mean specific heat one can hope to obtain information on this distribution function as with growing system size larger droplets will fit into the system. However, the droplets in our dimer model simulation seem to be dominated by the system boundaries. The number of configurations of lowest excitation energy that differ only on the boundaries from the ground-state configuration scales like the linear system size L , yielding a $1/L$ decay for the specific heat (instead of a growth from bulk droplets) to its asymptotic value. In fact, this scaling behavior is observed for the specific-heat data of our dimer model simulation, see Fig. 14. Indeed, low-lying excitations on the boundary can be easily identified. Consider a bond on the boundary that is occupied by a dimer in the ground state. A configuration that does not cover this very bond may remain unchanged on all the other bonds since simulations are done with open boundary conditions. The missing energy on the bond is the excitation energy, whose probability distribution, however, is nontrivial. The knowledge of this distribution would allow to calculate the finite-size scaling of the slope of the specific heat at $T_d=0$. Due to the simplicity of the boundary droplets the distribution could be computed with the dimer algorithm. The conditional probability that a bond is occupied given its random energy is just the probability $p(ij)$ introduced above

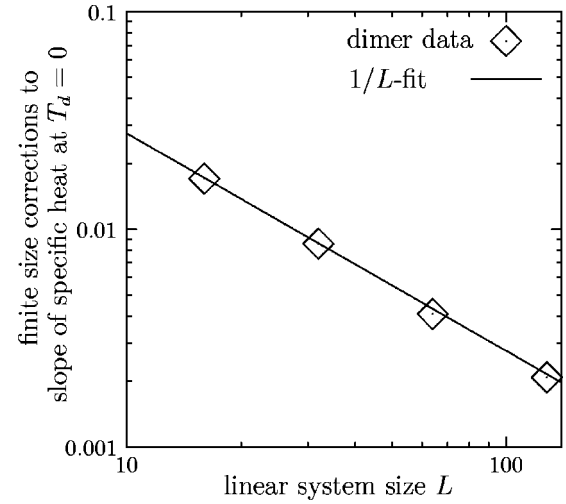


FIG. 14. Scaling of the slope of the dimer specific heat \bar{c}_d at $T_d=0$ with the system size.

in the calculation of the internal energy, see Sec. IV B. It can be easily obtained from the dimer algorithm. The distribution of the boundary droplet energies is then given by $p(ij)p(\text{occ})/p(E)$ with $p(\text{occ})$, $p(E)$ being the probabilities for the occupation and energy $\epsilon_{ij}=E$ of a bond, respectively.

The smallest droplet excitation in the bulk is likewise easily identified as the rotation of a plaquette that consists of two opposite dimers. The probability distribution for the energy difference of the two configurations is, however, not easily obtained. It is complicated by the condition that the two dimers before the flip must be part of the ground-state configuration. In the simulations, it should be stressed, statistics of droplet energies can in principle be measured systematically in the following straightforward procedure. For a given disorder configuration the ground-state dimer covering is determined. Then the energy of one arbitrary *occupied* bond in the bulk is set to infinity and the new ground state is determined. It will not contain the bond with infinite energy and hence have higher energy than the original ground state. The energy difference E together with the diameter ℓ of the nonoverlapping region of the two ground states is measured. The statistics of these pairs of values for many disorder realizations yield the distribution $p_\ell(E)$. Quantitative support of the scaling prediction of droplet theory is in reach considering the orders of magnitude over which the dimer model can be simulated.

V. SUMMARY AND DISCUSSION

In this paper we have compared recent exact replica Bethe *Ansatz* results for the planar line lattice with numerical simulations of the classical random bond dimer model. We found excellent agreement for a large set of disorder averaged thermodynamic quantities, namely the effective disorder renormalized elastic stiffness, the free energy, the internal energy, entropy, and the specific heat of the dimer model. Characteristics of the disorder distribution of thermodynamic quantities can also be obtained both from the Bethe *Ansatz* and from simulations and their agreement has explicitly been

shown for the variance and the skewness (third cumulant) of the free energy. The comparison thus confirms the replica Bethe *Ansatz* calculation of Ref. 11 and makes the $(1+1)$ -dimensional line lattice one of the few glassy systems for which the validity of a replica approach (without replica symmetry breaking) can be critically tested in detail. In the comparison, only one free parameter has been used which is the ratio of the short-scale regularization lengths of the continuous line model and the lattice constant of the discrete dimer model. The ratio is found to be consistently of the order of unity for all studied thermodynamic quantities. One term in the single-line free energy, first given in Ref. 24, could not be confirmed by the simulations, in consistency with numerical data of Ref. 31. It would be interesting to

relate the droplet excitations of the dimer or line system to the excitations of the related $SU(n)$ Fermi gas in the limit $n \rightarrow 0$. In view of the manifold links of dimer covering models to condensed-matter systems, especially of spin systems^{35–37} the link to the exactly solved disordered line-lattice model might prove useful in future applications.

ACKNOWLEDGMENTS

Interesting discussions with M. Kardar and S. Scheidl are gratefully acknowledged. This research was supported by the Deutsche Forschungsgemeinschaft (DFG) through an Emmy Noether grant (S.B. and T.E.) and by NSF Grant No. DMR-0049176 (A.T. and C.Z.).

-
- ¹K. Binder and A. Young, *Rev. Mod. Phys.* **58**, 801 (1986).
²T. Nattermann and S. Scheidl, *Adv. Phys.* **49**, 607 (2000).
³*Mesoscopic Quantum Physics*, edited by E. Akkermans, J.-L. Pichard, and G. Montambaux (North-Holland, Amsterdam, 1994).
⁴D.S. Fisher, *Phys. Rev. Lett.* **56**, 1964 (1986).
⁵M. Mezard and G. Parisi, *J. Phys. I* **1**, 809 (1991).
⁶D.S. Fisher and D.A. Huse, *Phys. Rev. B* **38**, 386 (1988).
⁷C. Zeng, A.A. Middleton, and Y. Shapir, *Phys. Rev. Lett.* **77**, 3204 (1996).
⁸C. Zeng, P.L. Leath, and T. Hwa, *Phys. Rev. Lett.* **83**, 4860 (1999).
⁹C.A. Bolle, V. Aksyuk, F. Pardo, P.L. Gammel, E. Zeldov, E. Bucher, R. Boie, D.J. Bishop, and D.R. Nelson, *Nature (London)* **399**, 43 (1999).
¹⁰M. Kardar, *Nucl. Phys. B* **290**, 582 (1987).
¹¹T. Emig and M. Kardar, *Nucl. Phys. B* **604**, 479 (2001).
¹²T. Emig and M. Kardar, *Phys. Rev. Lett.* **85**, 2176 (2000).
¹³T. Emig and S. Bogner, *Phys. Rev. Lett.* **90**, 185701 (2003).
¹⁴N. Elkies, G. Kuperberg, M. Larsen, and J. Propp, *J. Algebr. Comb.* **1**, 111 (1992).
¹⁵N. Elkies, G. Kuperberg, M. Larsen, and J. Propp, *J. Algebr. Comb.* **1**, 219 (1992).
¹⁶P.W. Kasteleyn, *Physica (Utrecht)* **27**, 1209 (1961).
¹⁷C.L. Henley, *J. Stat. Phys.* **89**, 483 (1997).
¹⁸L.D. Landau and E.M. Lifshitz, *Elasticity Theory* (Pergamon Press, Oxford, 1969).
¹⁹D.R. Nelson and H.S. Seung, *Phys. Rev. B* **39**, 9153 (1989).
²⁰V.L. Pokrovsky and A.L. Talapov, *Phys. Rev. Lett.* **42**, 65 (1979).
²¹P.G. de Gennes, *J. Chem. Phys.* **48**, 2257 (1968).
²²B. Sutherland, *Phys. Rev. Lett.* **20**, 98 (1968).
²³M. Takahashi, *Prog. Theor. Phys.* **44**, 899 (1970).
²⁴M. Kardar and D.R. Nelson, *Phys. Rev. Lett.* **55**, 1157 (1985).
²⁵J.M. Kim, M.A. Moore, and A.J. Bray, *Phys. Rev. A* **44**, 2345 (1991).
²⁶J.-P. Bouchaud and H. Orland, *J. Stat. Phys.* **61**, 877 (1990).
²⁷E. Brunet and B. Derrida, *Phys. Rev. E* **61**, 6789 (2000).
²⁸E.H. Lieb and W. Liniger, *Phys. Rev.* **130**, 1605 (1963).
²⁹N.N. Bogoliubov, *J. Phys. (USSR)* **11**, 23 (1947).
³⁰S.E. Korshunov and V.E. Dotsenko, *J. Phys. A* **31**, 2591 (1998).
³¹J. Krug, P. Meakin, and T. Halpin-Healy, *Phys. Rev. A* **45**, 638 (1992).
³²W. Press, B. Flanery, S. Teukolsky, and W. Vetterling, *Numerical Recipes in C*, 2nd ed. (Cambridge University Press, Cambridge, 1993).
³³D.S. Fisher and D.A. Huse, *J. Phys. A* **20**, 1005 (1987).
³⁴P.W. Anderson, B.I. Halperin, and C.M. Varma, *Philos. Mag.* **8**, 1 (1972).
³⁵M.E. Fisher, *J. Math. Phys.* **7**, 1776 (1966).
³⁶M. Kac and J.C. Ward, *Phys. Rev.* **88**, 1332 (1952).
³⁷R. Moessner and S.L. Sondhi, *Prog. Theor. Phys. Suppl.* **145**, 37 (2002).